

# Applying Taguchi methods for solvent-assisted PMMA bonding technique for static and dynamic $\mu$ -TAS devices

Yi-Chu Hsu · Tang-Yuan Chen

Published online: 22 May 2007  
© Springer Science + Business Media, LLC 2007

**Abstract** This work examines numerous significant process parameters in the solvent-assistant Polymethyl methacrylate (PMMA) bonding scheme and presents two Micro-total-analysis System ( $\mu$ -TAS) devices generated by adopting the optimal bonding parameters. The process parameters considered were heating temperature, applied loading, duration and solution. The effects of selected process parameters on bonding dimensions loss and strength, and subsequent optimal setting of the parameters were accomplished using Taguchi's scheme. Additionally, two  $\mu$ -TAS devices were realized using a static paraffin microvalve and a dynamic diffuser micropump. The PMMA chips were carved using a CO<sub>2</sub> laser that patterned device micro-channels and microchambers. The operation principles, fabrication processes and experimental performance of the devices are discussed. This bonding technique has numerous benefits, including high bonding strength (240 kgf/cm<sup>2</sup>) and low dimension loss (2–6%). For comparison, this work also demonstrates that the normal stress of this technology is 2–15 times greater than that of other bonding technologies, including hot embossing, anodic bonding, direct bonding and thermal fusion bonding.

**Keywords** PMMA bonding ·  $\mu$ -TAS · Microvalves · Micropumps · Taguchi's method

## 1 Introduction

Microfluidic devices have countless applications in areas such as analytical chemistry (Reyes 2002), biological applications (Lee 2001), pharmaceutical development (Kricka 1998), and chemical synthesis systems (Whitesides 2001). Compared with conventional macro-scale systems, these devices have numerous advantages, such as their compact size, great potential for system automation, reduced waste, increased precision and accuracy, and for providing fast analytical tools. A limit of these devices is that the commonly used fabrication methods (e.g., silicon dry etching) and materials (e.g., silicon, quartz or glass) are relatively expensive. Moreover, it is difficult to produce high-aspect-ratio (the ratio of feature height to lateral dimension) microstructures. Although this difficulty can be circumvented to a certain degree using reactive ion etching or anisotropic etching in single crystal silicon, these methodologies are often prohibitively expensive and slow, decreasing production rates of microfluidic devices. Furthermore, final assembly requires high temperatures, thereby precluding any chemical modifications of the substrate surface or inclusion of materials in fluidic networks prior to assembly.

Polymers as substrate materials conversely offer the advantages of low cost, chemical inertness, lightweight, volume fabrication with added benefits of disposability, bio-compatibility, optical clarity, non-fragility when handling and a wide variety of materials to choose from. Different polymers, such as polydimethylsiloxane (PDMS) (McDonald et al. 2000), polymethylmethacrylate (PMMA) (Muck 2004) and polycarbonate (PC), (Liu 2001) have been widely investigated for applications during microfluidic fabrication. Table 1 compares and summarizes the characteristics of silicon, glass and polymers.

---

Y.-C. Hsu (✉) · T.-Y. Chen  
Department of Mechanical Engineering,  
Southern Taiwan University of Technology,  
Yung Kang City, Tainan County, Taiwan  
e-mail: yichu@mail.stut.edu.tw

**Table 1** Comparison of silicon, glass and polymers for microfluidic devices

	Silicon	Glass	Polymer
Cost	High	High	Low
Optical clarity	Bad	Good	Good
High-aspect-ratio structure	Slow	Difficult	Easy
Bio-compatibility	Bad	Bad	Good
Fragility for handling	Bad	Bad	Good

Bonding and sealing polymer-based microfluidic devices is difficult without changing or destroying the integrity of patterned microstructures. A number of bonding approaches have been developed, such as adhesive bonding (Wijngaart et al. 2001; Kim and Xu 2004; Martin et al. 1998), hot embossing (McGraw et al. 2005; Kameoka et al. 2001), solvent bonding (Glasgow 1999), microwave welding (Lei et al. 2004; Yussuf et al. 2005) and resin-gas injection bonding (Lai 2004). This study presents a new bonding approach that does not use specific equipment, such as a microwave cavity or hot embossing machine, and does not leave an interfacial layer of significant thickness. Furthermore, channel dimension loss during sealing is efficiently reduced to only 2–6%, and, therefore, the configuration of microchannels and microchambers is not altered. This technique used solvents like ethanol, methanol, and isopropanol to bond two PMMA chips with micro-patterns. The possible bonding mechanism has been discussed by the observation of FTIR spectra (Limm and Hong 1990). It shows disappearance of the C=O stretching band of the Bulk-TB for PMMA in Alcohol and its analogues dissolved in alcohols suggests an unusually strong, yet reversible, interaction between the ester carbonyl group and hydroxyl group of alcohols. They have suspected either a very strong hydrogen bond type interaction or an outright reaction involving the carbonyl group. However, no satisfactory explanation has been found.

This study presents a promising approach for achieving a simple Micro-electrical–mechanical System (MEMS) fabrication process for compatible bonding of microfluidic polymer substrate using solvents which do not cause marked deformation of patterned microstructures. Moreover, to assess the effects of applying this technique to MEMS technology, two microfluidic devices were designed, fabricated, and tested: one device is a static component of microvalves, and the other is a dynamic device of micropumps. The performance of these devices was experimentally demonstrated.

## 2 Taguchi analysis of PMMA bonding process

To evaluate the bonding processes, this study analyzed bonding dimension loss and bonding strength. Small dimension loss and high bonding strength are important for plastic bonding technique put on MEMS devices. In addition, three kinds of bonding strength were measured: shear strength, normal strength and sealing strength. The normal bonding strength was tested to compare solvent-assisted bonding method with other plastic bonding techniques. The sealing strength was evaluated to ensure the proposed bonding method is proper to use for the MEMS community.

Taguchi methods were applied for the analysis of the dimension loss and shear bonding strength. Four process parameters were chosen: heating temperature, applied loading, duration and solution. Each parameter was analyzed at three levels. The  $L_9(3^4)$  orthogonal array (OA) was adopted (the first four columns in Table 2). Table 3 presents the parameters and with their values at selected levels.

### 2.1 Bonding dimension loss

Bonding dimension loss is an issue for the most frequently utilized plastic bonding technique—hot embossing bonding.

**Table 2** OA, experimental data and SN ratios

Specimen no.	A	B	C	D	Experimental data ( $\mu\text{m}$ )		Dimension loss ratio (%)	SN ratio (dB)
					$y_1$	$y_2$		
					1	1		
2	1	2	2	2	8	10	5	-19.14
3	1	3	3	3	3	5	2	-12.30
4	2	1	2	3	4	6	3	-26.86
5	2	2	3	1	8	6	4	-22.11
6	2	3	1	2	8	10	5	-25.80
7	3	1	3	2	14	9	6	-21.41
8	3	2	1	3	2	6	2	-13.01
9	3	3	2	1	1	9	3	-16.13

**Table 3** Process parameters and their values at three levels

Parameter destination	Process parameters	Level 1	Level 2	Level 3
A	Heating temperature (°C)	60	80	100
B	Applied loading (kg/cm <sup>2</sup> )	0.05 (0.7112 psi)	0.15 (2.133 psi)	0.25 (3.556 psi)
C	Duration (min)	5	7	9
D	Solution	Methanol	Ethanol	Isopropanol

Comparison with the macro-scale samples, the dimension loss is more significant for micro-plastic devices due to their small geometries. Using Taguchi models, this study attempted to identify the optimum parameters for smallest bonding depth loss using the proposed technique.

Based on OA on Table 2, nine pairs of PMMA chips were bonded. First of all, one PMMA chip was carved by CO<sub>2</sub> laser (Universal Laser System Inc, M300) to form the pattern shown in Fig 2(a). Second, another PMMA without any pattern was dip into solvent and pull out immediately for the bonding process. Figure 1 presents the cross section of a bounded specimen. Each specimen has two PMMA chips. Hot plates were put on the top and bottom of the PMMA specimen to control temperature, applied loading and duration. The PMMA with pattern is the bottom one. It was cut at the location AA' and BB' as shown in Fig. 2(a), after the bonding process. The cross section is demonstrated in Fig. 2(b). Before the bonding process, the cross section of the bottom PMMA chip is 500 μm wide and 200 μm deep. The channel depths were measured again using an optical microscope after the bonding process. The depth differences before and after bonding are  $y_1$  and  $y_2$  at locations of AA' and BB', respectively (Table 2).

Bonding depth loss is a “the-smaller-the-better” characteristic. Consequently, the signal-to-noise ratio (SN) for that response was used and calculated using Eq. 2-1. The last column in Table 2 presents the SN ratios.

$$(SN \text{ ratio}) = -10 \log \left[ \frac{1}{2} \sum_{i=1}^n y_i^2 \right] \tag{2-1}$$

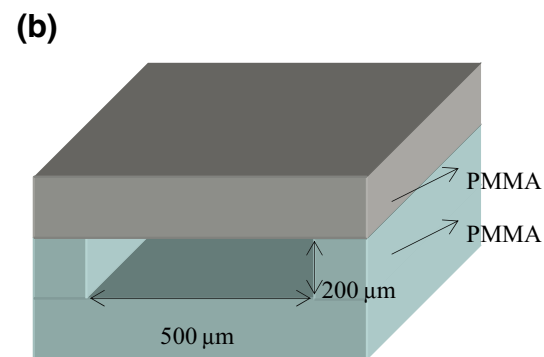
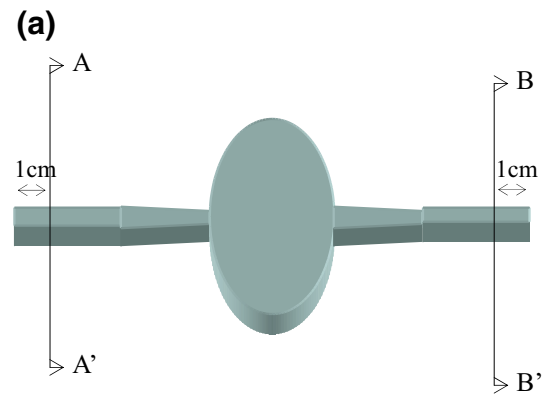
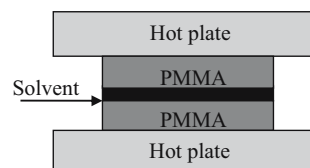
where  $y_i$  is experimental data (Table 2) and  $n$  is the measuring number (2 in this case).

Table 4 and Fig. 3 present the summation of SN ratios for various factors at different levels. For example, A1 means factor A at level 1 and the value of -15.86 is the

average of the SN ratio of specimen no. 1, 2 and 3 in Table 2. Table 4 also presents the main effects for SN data. The main effects are the difference between the maximum and minimum SN ratios of the three levels for the same factor. For instance, the main effect of factor A is the difference between level 1 (maximum value) and level 2 (minimum value).

It is clear from Fig. 3 and Table 4 that parameter A is more prominent than the other parameters. The size of the main effect value is positively correlated with the prominence of parameters. Parameters D, B and C are the subsequent significant parameters. It is also clear that bonding depth loss is minimum at the first level for parameters A and C, and at the third level for parameters B and D (Table 4). As a result, the SN ratio analysis indicates that the combination of A1 (heating temperature 60°C), B3

**Fig. 1** PMMA to PMMA bonding using solvent assistant process



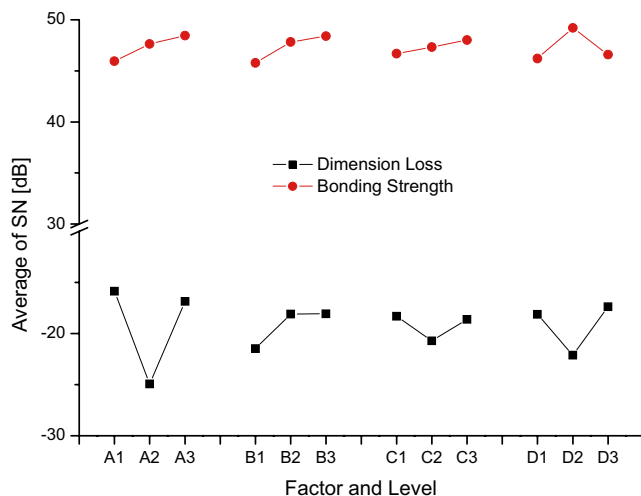
**Fig. 2** (a) Pattern of bonded PMMA pairs. (b) Cross section view of locations A-A' and B-B' at (a)

**Table 4** Summation of SN ratios at the different levels and their main effects

Factor	Level 1	Level 2	Level 3	Main effect
A	-15.86	-24.92	-16.85	9.07
B	-21.47	-18.09	-18.08	3.39
C	-18.31	-20.78	-18.61	2.39
D	-18.12	-22.12	-17.39	4.73

(applied loading of  $0.25 \text{ kg/cm}^2$ ), C1 (duration of 5 min) and D3 (isopropanol) was the best for reducing depth loss during the solvent-assisted bonding technique.

Based on these experimental results, a low temperature and short duration resulted in small depth loss. Moreover, this study determined that isopropanol is least easily to dissolving PMMA during the experimental procedure and, therefore, yields the smallest bonding loss. However, it is likely least reasonable that increased loading results in a small depth loss. In our opinion, there are three reasons to cause this result. First of all, the applied loading is usually between  $30$  and  $180 \text{ kg/cm}^2$  for PMMA bonding by conventional hot embossing (Mekaru et al. 2004; Qi et al. 2002). However, our method only needs  $0.05\sim 0.25 \text{ kg/cm}^2$ . The range of our loading is much smaller than the conventional method, because the bonding mechanism of the proposed method mostly relies on the solvent, not the applied loading. Therefore, the applied loading of the applied range is not big enough to influence the bonding effects. In addition, this issue does show in the experiments. For example, B2 ( $0.15 \text{ kg/cm}^2$ ) and B3 ( $0.25 \text{ kg/cm}^2$ ) demonstrate approximately the same SN ratios ( $-18.09$  and  $-18.08$ ) in Table 4. Secondly, the experimental data  $y_1$  and  $y_2$  in Table 3 were observed in microscope. Usually, the shape of microchannel after bonding is not as rectangular/

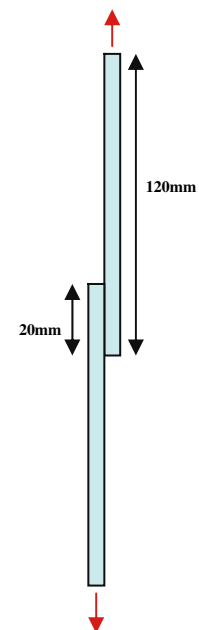
**Fig. 3** SN ratios of various parameters at the different levels for bonding strength and dimension loss tests

perfect as shown in Fig. 2(b) and a manual/artificial judgment is required to calculate  $y_1$  and  $y_2$ . This manual reading cannot be avoided and could cause some difference in the experimental result. Finally, the flatness of PMMA chips and hot plates is probably not good enough to cause an uneven loading during the experiments. We think these three reasons (the applied loading is not significant for our bonding technique, inevitable manual reading could cause tiny data error, and the flatness of chips is not perfect) could generate such result.

In addition, Table 3 demonstrates the dimension loss ratio is 2–6%. For comparison, this study also utilized hot embossing to bond two PMMA chips under the same conditions (Fig. 2). The parameters for the hot embossing machine are temperature of  $140^\circ\text{C}$ , loading pressure of  $40 \text{ kg/cm}^2$  and duration of 1 min. Dimension loss ratio was 30% for this case.

## 2.2 Bonding strength

Three tests were performed to assess bonding strength. The first test used the Taguchi method to analyze optimal bonding parameters. Shear stress measured was the first bonding strength estimated using an ultimate tensile machine (Tokyo, RU-30). The second test compares bonding strength of normal stress using the proposed technique and other techniques such as hot embossing, anodic bonding, direct bonding and thermal fusion. Normal stress was measured using another ultimate tensile machine (MTS Sintech 5/G). The final test estimated the sealing strength of the solvent-assisted bonding method. Two

**Fig. 4** Schematic diagram of PMMA specimen for shear stress testing

**Table 5** OA, experimental data and SN ratios for bonding strength test

Specimen no.	A	B	C	D	Experimental data (kgf/cm <sup>2</sup> )		SN ratio (dB)
					y <sub>1</sub>	y <sub>2</sub>	
1	1	1	1	1	126	146	42.60
2	1	2	2	2	264	255	48.28
3	1	3	3	3	216	230	46.95
4	2	1	2	3	194	176	45.31
5	2	2	3	1	251	234	47.68
6	2	3	1	2	306	321	49.92
7	3	1	3	2	284	311	49.44
8	3	2	1	3	224	255	47.53
9	3	3	2	1	260	264	48.37

optimal bonding combinations recommended by Taguchi method analysis based on minimum dimension loss and maximum shear stress were evaluated.

2.2.1 Taguchi method

The ultimate tensile machine (Tokyo, RU-30) was utilized to measure shear stress and to separate two bonded PMMA plates. Two pure PMMA plates (120×32×5 mm) with bonding area of 20×32 mm were placed in the ultimate tensile machine (Fig. 4). Table 5 presents measurement results.

The bonding strength of the Taguchi method is a “larger-the-better” problem. Consequently, the SN ratio was calculated using Eq. 2-2. The final column in Table 5 presents SN ratios.

$$SN \text{ ratio(dB)} = -10 \log \left[ \frac{1}{2} \sum_{i=1}^n \frac{1}{(y_i)^2} \right] \tag{2-2}$$

where  $y_i$  is experimental data (Table 5) and  $n$  is the measurement number (2 in this case).

Table 6 and Fig. 3 present summations of SN ratios for various parameters at different levels. For example, A1 means factor A at level 1 and the value of 45.94 is the average of the SN ratio of specimen no. 1, 2 and 3 in Table 5. Table 6 also presents the main effects for SN data for various parameters.

**Table 6** Summation of SN ratios at the different levels and their main effects for bonding test

	Level 1	Level 2	Level 3	Main effects
A	45.94	47.64	48.45	2.50
B	45.79	47.83	48.41	2.63
C	46.68	47.32	48.02	1.34
D	46.21	49.21	46.60	3.00

Parameter D is more prominent than the other parameters (Fig. 3 and Table 6). Parameters B, A and C are the subsequent significant parameters. Shear strength is maximal at the third level for parameters A, B and C, and the second level for parameter D (Table 6). Consequently, SN ratio analysis indicates that the combination of A3 (heating temperature 100°C), B3 (applied loading 0.25 kg/cm<sup>2</sup>), C3 (duration 9 min) and D2 (ethanol) were the best levels for increasing the strength of the solvent-assisted bond. Based on the experimental results, a high temperature, great loading and extended duration increased the bonding strength. Additionally, ethanol dissolved PMMA best and, accordingly, generates the greatest bonding strength.

2.2.2 Bonding technique comparison

To compare the proposed bonding technology with other technologies regularly used in the MEMS communities, normal stress was measured by another ultimate tensile machine (MTS, Sintech 5/G). Specimen dimensions were 2.5 cm×2.5 cm×1 mm (Fig. 5). The operational conditions for the ultimate tensile machine were maximum output

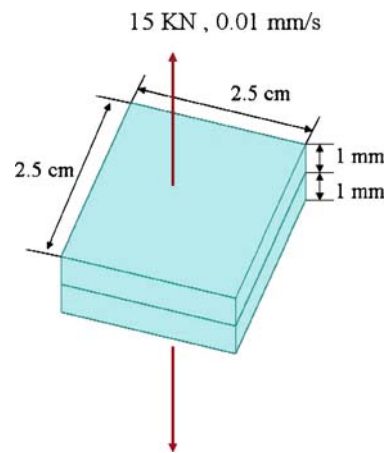


**Fig. 5** PMMA specimen for normal stress

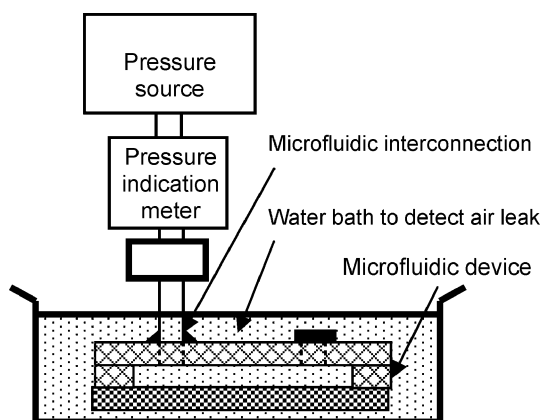
**Table 7** Experimental comparison of different bonding techniques

Bonding process	Hot embossing	Anodic bonding	Direct bonding	Thermal fusion bonding	Solvent assistant bonding
Bonding materials	PMMA-PMMA	Silicon-Pyrex	PDMA-glass	Glass-glass	PMMA-PMMA
Bonding conditions	140°C 40 kg/cm <sup>2</sup> 1 min	475°C 1,000 V	Room temperature	670°C	60°C 0.25 kg/cm <sup>2</sup> 5 min
Peak load (kgf)	41.61	28.95	12.04	83.38	179.3

loading of 15 kN and pulling speed of 0.01 mm/s. The following five bonding technologies were introduced during testing: hot embossing, anodic bonding, direct bonding, thermal fusion and solvent-assisted bonding. Parameters of A1 (60°C), B3 (0.25 kg/cm<sup>2</sup>), C1 (9 min) and D3 (isopropanol) were applied to the PMMA specimen with the solvent-assisted bonding technique. Table 7 presents the applied materials, bonding conditions and peak load during testing. Experimental results demonstrate that normal bonding strength of the solvent-assisted technique is 2–15 times greater than that of other techniques.

### 2.2.3 Sealing strength

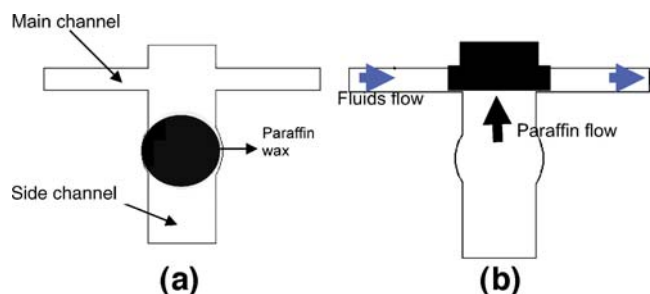
Based on the experimental data (Table 5), the average amount of bonding shear stress on two flat PMMA chips was 240 kgf/cm<sup>2</sup>. The normal stress for the proposed bonding technique was 179.3 kgf. To estimate further the sealing condition of bonding chips suitable for microfluidic applications, another test was performed (Fig. 6). One pair of bonded PMMA specimens with a microchannel and two inlet/outlet holes was immersed in a water bath. First, the inlet hole on the left connected to a pressure source with a pressure indicator meter. Then, air was pumped into the specimen through the left inlet hole. A bubble coming out of the right outlet hole confirmed that the connection to the pressure source was appropriate. Furthermore, the microchannel and inlet/outlet holes were not clogged. Next, the outlet hole on the right side was closed and pressure was

**Fig. 6** Experimental setup for sealing strength measurement

applied to the specimen until it leaked. The best combinations of process parameters for smallest depth loss (A1, B3, C1 and D3) and greatest bonding strength (A3, B3, C3 and D2) were estimated. Both parameter sets were capable of holding until pressure reached 100 psi. Based on the sealing strength test results, both combinations of process parameters were adequate for application on micro total analysis systems. Thus, the combination of minimum bonding depth loss was utilized next to assist the solvent bonding technique for two plastic microdevices: one static microvalve and one dynamic micropump.

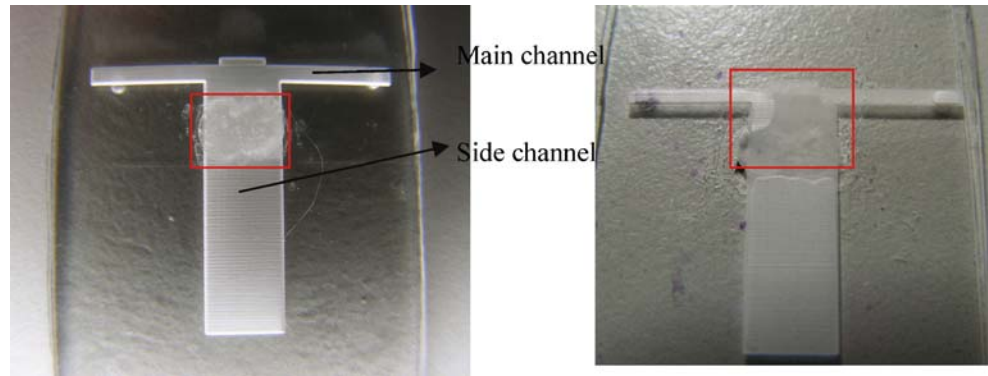
### 3 Application on a paraffin microvalve

To evaluate bonding performance, a paraffin microvalve was first designed, fabricated and tested. A PMMA chip was carved to form a T-shaped channel with a vertical side channel and a transversal main channel (Fig. 7(a)) using a CO<sub>2</sub> laser (Universal Laser System, Inc., M300). The applied power, speed and resolution of the laser operation were 45%, 60% and 1,000 DPI, respectively. The depth of carved channels, width of the top transverse main channel and that of the middle vertical side channel were 200 μm, 1 mm and 5 mm, respectively. Next, one clean PMMA chip—with two inlet/outlet holes on the primary channel for liquid and one middle hole on the side channel for paraffin—was bonded to the carved PMMA chip using the proposed solvent-assisted method with parameter of A1, B3, C1 and D3.

**Fig. 7** (a) schematic diagram of T-shape channel with paraffin wax before the main channel blocked. (b) schematic diagram of paraffin blocking fluid



**Fig. 8** Photo of the microvalve before paraffin melting  
**Fig. 9** Photo of the microvalve after paraffin melting



The paraffin wax (Sigma-Aldrich 76228, melting point 44–46°C) has carbon number of 18-30 and a high volume expansion effect (10–30%) when temperature increases are small. As soon as the paraffin was placed into the side channel, the paraffin hole was sealed. During the following step, the PMMA device was placed on a hotplate with a temperature of 53°C. Within 2 min, the paraffin melted and flowed into the top primary channel owing to capillary force. Consequently, the flowing liquids in the primary channel were blocked by the paraffin (Fig. 7(b)). Figures 8 and 9 present photos of the T-shaped channel before and after heating. The location of the paraffin in the side channel initially and the primary channel eventually indicates that an active microvalve was achieved using this approach. This device can be applied easily to disposable plastic microchips to alter sample flow directions.

#### 4 Application on a diffuser micropump

##### 4.1 Principle of the pumping operation

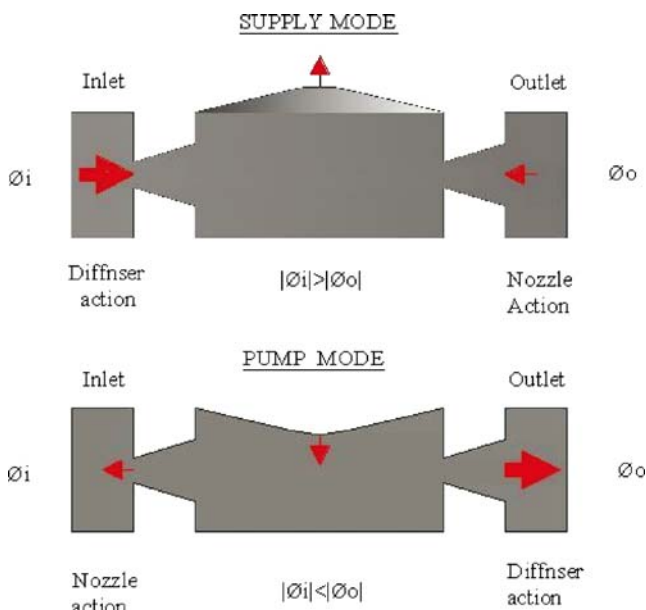
The diffuser micropump consists primarily of two diffuser elements connected to a fluid cavity volume with an oscillating diaphragm (Fig. 10). With correctly designed diffuser elements, the flow pressure drop in the diffuser direction is lower than that in the nozzle direction. Therefore, more fluid flows through the inlet element than that flowing through the outlet element during supply mode, and more fluid flows through the outlet element than that through the inlet element during pump mode. As a result, the net flow is from the inlet to the outlet.

##### 4.2 Design

Figure 11 presents pump dimensions. The chamber diameter, channel length and diffuser degree of the plastic micropump in PMMA are 6 mm, 5.5 mm and 5°, respectively.

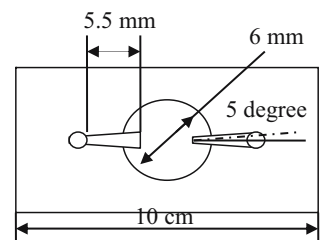
##### 4.3 Fabrication process

The micropump consists of two parts: a 1-mm-thick PMMA, and a commercially available bulk PZT chip (T107-H4E-602, Piezo Systems, Inc.). Figure 12 shows the microfabrication process for the PMMA chip. First, mask design was drawn using CorelDRAW11. Then, the



**Fig. 10** Schematic drawings of the supply and pumping modes of a diffuser micropump

**Fig. 11** Design of plastic micropump



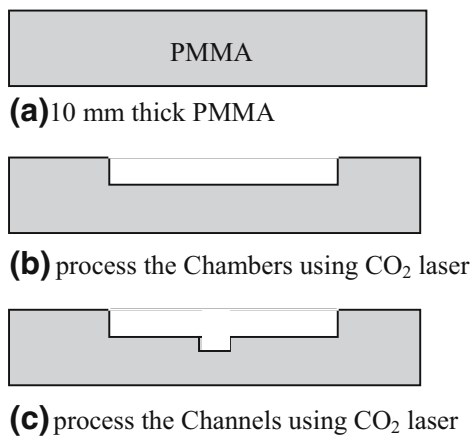


**Fig. 12** The microfabrication process of plastic micropumps using CO<sub>2</sub> laser

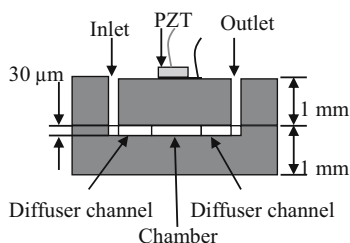
patterns of micropumps were carved on 1 mm PMMA chip using a CO<sub>2</sub> laser (M-300, Laser Systems, Inc.).

The pump outlet and inlet holes were drilled through the PMMA using diamond bits. The bonding of PMMA to PMMA was performed using the proposed solvent-assisted technique with parameters A1, B3, C1 and D3. A 6-mm<sup>2</sup> piezoelectric element with a thickness of 191 mm was attached to the PMMA chip using silver epoxy. Figure 13 presents the pump cross section and dimensions. The inlet and outlet tubes, and an electric connector were fixed onto the device by epoxy. Figure 14 presents the finished diffuser micropump.

## 5 Experiments and results of micropumps

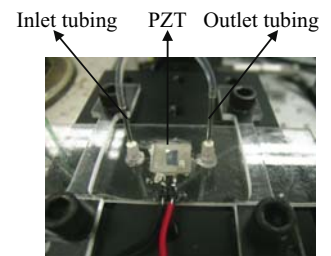
### 5.1 Experimental setup

Figure 15 shows a schematic of the experimental setup. Briefly, five instruments were utilized for pump performance tests: function generation (Motech, FG 503), microbalance (Sartorius, BL 120S), power amplifier (Piezotronics, PCB790), digital oscilloscope (Tektronix, TDS2014) and fiber-optical measurement system (MTI Instruments, MTI 2000). The system started with an electric signal distributed by the function generator. The signal was amplified and



**Fig. 13** The schematic diagram of the micropump

**Fig. 14** The photo of finished plastic micropump during testing



transformed to bulk PZT by the power amplifier. The PMMA membrane of the pump vibrated when a driving signal was generated. Additionally, the fiber-optical measurement system served as a displacement sensor for monitoring the dynamic performance of the micropump. All signals from the function generation, power amplifier and fiber-optical measurement system were recorded by the digital oscilloscope. Finally, flow rates of fluid were estimated based on the position of fluid in the outlet tube. The working fluid was DI water.

### 5.2 Pump performance

The pump frequency response was measured by the fiber-optic probe as peak displacement of the center of the driving piezoelectric actuator, and as a function of frequency at a fixed driving voltage when the pump system was filled with DI water. Figure 16 presents the displacement of the PMMA driven by the PZT chip at a fixed voltage of 100 V and frequencies of 100–1,000 Hz. The maximum displacement of the membrane was 0.1941 mm (peak-to-peak) at 150 Hz, which was the first device resonance.

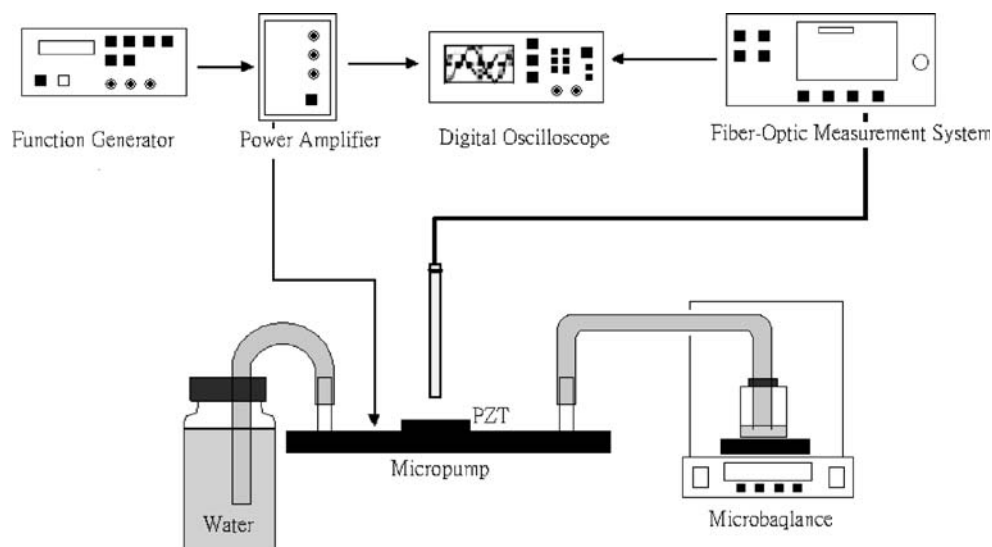
Figure 17 presents the flow rate vs. voltage at 100 Hz while electric voltages were 100–180 V<sub>PP</sub>. The flow rate was approximately proportional to voltage. The maximum flow rate was 14.3 ml/min at a voltage of 180 V<sub>PP</sub>.

## 6 Conclusions and future works

This study presented a new and very promising scheme for achieving a simple MEMS fabrication process-compatible bonding for microfluidic polymer substrates using solvents. Dimension loss and strength of the bonded PMMA chips were assessed using Taguchi's approach according to the effects of heating temperature, applied loading, duration and solution. To minimize bonding dimension loss, parameters A1 (heating temperature of 60°C), B3 (applied loading of 0.25 kg/cm<sup>2</sup>), C1 (duration of 5 min) and D3 (isopropanol) were adopted. Additionally, the combination of A3 (heating temperature of 100°C), B3 (applied loading of 0.25 kg/cm<sup>2</sup>), C3 (duration of 9 min) and D2 (ethanol)



**Fig. 15** Schematic drawing of the experimental setup



was best for increasing bonding strength during the solvent-assisted bonding technique. Moreover, this study compared normal stress of solvent-assisted bonding with that of hot embossing, anodic bonding, direct bonding and thermal fusion. These techniques are commonly used in MEMS devices. Experimental results verified that normal bonding strength of the solvent-assisted technique is 2–15 times greater than that achieved using the other techniques. Finally, sealing strength was measured to ensure that the bonding technique was suited to  $\mu$ -TAS applications. Although the parameters for minimum dimension loss and maximum strength differed considerably, the sealing strengths of the two cases were both greater than 100 psi.

To investigate the effects of applying this technique on MEMS technology, two microfluidic devices were created: one was a static component of a microvalve, and the other one was a dynamic micropump device. When the proposed bonding technique was applied to the microvalve, melted

paraffin spilled into the primary channel and blocked the microchannel, demonstrating that the solvent-assisted bonding technique could be applied to static microdevices.

When the proposed bonding technique was applied to a PMMA diffuser micropump, experimental results demonstrated that maximum flow rate, 14.3 ml/min, was located at 100 Hz at a voltage of 180 V<sub>pp</sub>. Maximum membrane displacement was 0.19 mm (peak-to-peak) at 150 Hz, which is the first device resonance.

Plastic is promising to apply to BioMEMS devices. Lee (2001) has used hot embossing methods to construct plastic microchips which can separate and detect DNA. We are working on different approaches, such as protein chips (Keng et al. 2006) and microdosing system which supplies small amount of medicine into patients constantly. We recently successfully utilized 4, 4-DTBA as a monolayer of the protein chip based on gold surface. The results show that 4, 4-DTBA was able to generate a more uniform monolayer

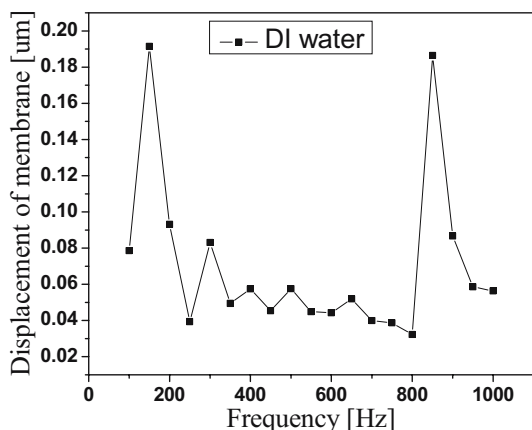


**Fig. 16** The displacement of membrane versus driving frequency at 100 V<sub>pp</sub>

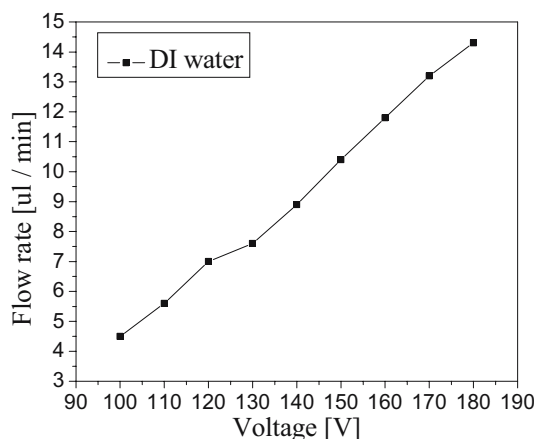


**Fig. 17** Flow rate versus voltage at a fixed driving frequency of 100 Hz

than 11-MUA (11-mercaptoundecanoic acid), which is conventionally used. Therefore, the SAM (self-assembled monolayer) of 4, 4-DTBA can be used as a monolayer to fabricate the protein chip. The monolayer was synthesized on gold layer above silicon substrate previously and now it's implemented on gold layer upon PMMA chips with microchannels to transport microfluidics. In addition, a peristaltic micropump based on two PMMA chips which are bonded by this proposed method is developing for microdosing system.

**Acknowledgments** The authors would like to thank the National Science Council of the Republic of China, Taiwan, for financially supporting this research under Contract No. NSC 95-2212-E-218-055. National Nano Device Laboratories, Center for Micro/Nano Technology Research and Nanotechnology Research Center in Southern Taiwan University of Technology are also commended for fabrication and measurement support. Dr. W. C. Sue from Department of Mechanical Engineering in Southern Taiwan University of Technology is appreciated for kindly providing technical support on bonding strength measurement.

## References

- I.K. Glasgow, D.J. Beebe, V.E. White, *Sensors Mater.* **11**, 269–278 (1999)
- J. Kameoka, H.G. Craighead, H. Zhang, J. Henion, *Anal. Chem.* **73** (9), 1935–1941 (2001)
- H.-K. Keng, Y.-C. Hsu, L.-S. Jang, in *5th IEEE International Conference on Sensors, A3L-F1*, Daegu, Korea, 22–25 October 2006
- J. Kim, X. Xu, Laser-based fabrication of polymer micropump. *J. Microlithogr. Microfabr. Microsyst.* **3**(1), 152–158 (2004)
- L.J. Kricka, *Clin. Chem.* **44**, 2008–2014 (1998)
- S. Lai, X. Cao, L.J. Lee, *Anal. Chem.* **76**, 1175–1183 (2004)
- G.B. Lee, S.H. Chen, Y.H. Lin, *Sens. Actuators, B* **75**, 142–148 (2001)
- K.F. Lei, S. Ahsan, N. Budraa, W.J. Li, J.D. Mai, *Sens. Actuators, A, Phys.* **114**(2–3), 340–346 (2004)
- W. Limm, S.H. Hong, *Polymer Preprints*, **31**(2) 613–614 (1990)
- Y. Liu, *Anal. Chem.* **73**, 4196–4201 (2001)
- M.P. Martin, D.W. Matson, W.D. Bennett, *Proc. SPIE* **3515** 172–176 (1998)
- J.C. McDonald, D.C. Duffy, J.R. Anderson, D.T. Chiu, H. Wu, O.J.A. Schueller, *J.M. Electrophoresis* **21**, 27–40 (2000)
- G.J. McGraw, R.V. Davalos, J.D. Brazzle, J. Hachman, M.C. Hunter, J. Chames, G.J. Fiechtner, E.B. Cummings, Y. Fintschenko, B.A. Simmons, in *Progress in Biomedical Optics and Imaging—Proceedings of SPIE*, vol. 5715. Micromachining and Microfabrication Process Technology, vol. X, (2005) pp. 59–68
- H. Mekar, T. Yamada, S. Yan, T. Hattori, *Microsyst. Technol.* **10**(10), 682–688 (2004)
- A. Muck Jr., *Anal. Chem.* **76**, 2290–2297 (2004)
- S. Qi, X. Liu, S. Ford, J. Barrows, G. Thomas, K. Kelly, A. McCandless, K. Lian, J. Goettert, S.A. Soper, *Lab Chip* **2**, 88–95 (2002)
- D.R. Reyes, D. Iossifidis, P.-A. Auroux, A. Manz, *Anal. Chem.* **74**, 2623–2636 (2002)
- G. Whitesides, A. Stroock, *Phys. Today* **54**, 42–48 (2001)
- W. van der Wijngaart, P. Nilsson, P. Enoksson, G. Stemme, H. Andersson, *Sens. Actuators, B, Chem.* **72**(3), 259–265 (2001)
- A.A. Yussuf, I. Sbarski, J.P. Hayes, M. Solomon, N. Tran, *J. Micromechanics Microengineering* **15**(9), 1692–1699 (2005)